Hindawi
Shock and Vibration
Volume 2020, Article ID 2137945, 10 pages
https://doi.org/10.1155/2020/2137945

Research Article

Experimental Study and Damage Effect Analysis of Concrete Structures under the Combined Loadings of Penetration and Explosion

Hao Geng,[1,2] Hao Lu,[1] Shanzheng Sun,[1] Songlin Yue,[1] Chunming Song,[1] and Shufang Feng[3]

[1]*State Key Laboratory of Disaster Prevention and Mitigation of Explosion and Impact, Army Engineering University of PLA, Nanjing 210007, China*
[2]*The No. 95979th Troop of PLA, Shenyang 110000, China*
[3]*The No. 32395th Troop of PLA, Shenyang 110000, China*

Correspondence should be addressed to Hao Lu; lh829829@163.com

Received 23 January 2020; Accepted 18 May 2020; Published 30 May 2020

Academic Editor: Isabelle Sochet

The penetration-explosion warhead is one of the most effective weapons for use against concrete structures. In order to study the phenomena and results for concrete damage caused by the combined effects of penetration and explosion, field experiments were performed on damaged concrete targets with different penetration speeds and explosive charges. The damage to the targets was analyzed, the causes were determined, and prediction methodologies were developed. Dimensional analysis was used to fit experimental results, a formula for calculating the damage depth and volume was proposed, and the dependence of the damage depth and volume on the aspect ratio of the explosive (or charge) and the kinetic energy of bullet penetration were determined. For a given projectile size and quantity of explosives, the damage depth and volume of the concrete target increase with the increasing projectile impact coefficient, but this trend gradually decreases. This observation can also provide a reference for the optimal design of penetration-explosion warheads, exhibiting the desired performance-price ratio.

1. Introduction

With the continuous development of penetration weapons for modern warfare, the antiexplosion capabilities of buildings or facilities with significant strategic value have received increasing attention. As an essential building material, concrete is widely used in the construction of various buildings or facilities [1], and the penetration-explosion warhead is one of the most effective weapons used against concrete structures. Its combined damage effects cause the blast side of the structure to be damaged and the rear side to collapse, causing severe damage to the building structure and personnel inside [2–4]. Therefore, it is of great importance to study the combined loadings due to penetration and explosion and their effects on concrete structures [5].

Research on the dynamic response of concrete structures under the combined damage of penetration and explosion primarily involves studying the process of projectile penetration and the process of the explosion within the context of the initial penetration damage. Although there is considerable literature describing the damage effects of penetration or explosion on concrete structures, there are few studies on the combined effects of penetration and explosion.

In the study of concrete penetration damage, Frew et al. [6] found that when the ratio of the target diameter to the impact body diameter was significant, penetration depth and projectile body overload were not significantly affected, but the surface damage volume was significantly affected. Xue et al. [7] conducted an experiment comparing corundum-rubble concrete (CRC) and reinforced concrete and proposed an improved Taylor model to predict the penetration depth into CRC targets. Xue et al. [8] established an engineering calculation model based on the surface splitting mechanism and rigid kinematic equations in order to study

the effects of oblique angle and angle of attack on projectile penetration. Zhang et al. [9] developed a new method to predict the real-time penetration depth of ogive-nose projectiles into concrete targets based on acceleration data measured in penetration tests involving ogive-nose projectiles and semi-infinite concrete targets. Zhang et al. [10] describe an in-depth investigation designed to identify critical effective properties related to the penetration depth of small caliber nondeformable projectiles in cement-based materials across a wide range of compositions and material properties. Liu et al. [11] carried out experiments on the impact of medium carbon steel long-rod projectiles on concrete targets and studied the impact behavior of projectiles and concrete targets with different impact velocities.

In the studies of concrete explosion damage, Cofer et al. [12] created a finite element model for prestressed concrete beams and studied the effect of blast loads on the structure with two explosion tests. Fu and Zhang [13] studied the damage to the free surface of a reinforced concrete target subjected to an internal explosion load. Li and Hao [14] studied the damage mode for reinforced concrete slabs under aerial initiation conditions, and Zhang and Wang [15] studied the antiexplosion performance of concrete gravity dams under the impact of underwater explosion shocks. Rabczuk et al. [16] used field tests and numerical simulations on concrete slabs of different thicknesses and initiated explosive contact to compare the diameters and depths of craters on the front and back of concrete targets.

There are basically two kinds of treatment methods for research on the explosion resulting after the projectile penetrates the concrete structure: (1) burst the explosive directly inside the concrete for detonation or (2) place the explosive inside a shot hole in the concrete and do not block the shot hole. Leng et al. [17] used method (1) to study the dynamic response of cavity formation and developed predictive rules for the concrete structure under the effect of internal explosion load, and Lai et al. [18] studied the failure characteristics of super-strength concrete under conditions of different burial depths and different loadings. Yang and Wang [19] used method (2) with field experiments and numerical simulations to develop a suitable algorithm for numerical simulation of explosion problems in concrete dielectric targets, and Zhang et al. [20] studied the critical collapse thickness and the corresponding critical charge for a concrete target. It is noteworthy that none of the above studies considered the penetrating effect of the projectile.

In practice, due to the randomness in penetration speed, the depth of the explosion (penetration depth) often exhibits considerable uncertainty; this makes it difficult to evaluate the situation accurately, and the ultimate damage effect cannot be accurately judged. On one hand, if the penetration speed is very slow, the explosion point will be extremely shallow, and the explosive energy of the charge will be released into the air. The damage area on the blast side is small, typically consisting of visible pits, and the effect on the rear side is not apparent. On the other hand, if the penetration speed is very high, the explosion point will be extremely deep and the projectile will explode inside the concrete medium to form a gourd pit. The area of damage on the surface layer is then relatively small; although some bulges and cracks will be formed, they often do not contribute significantly to pit opening. Only the appropriate penetration speed will allow the penetration-explosion warhead to inflict maximum damage. In addition, the charge and aspect ratio are also important factors affecting the power of the penetration-explosion warhead, and differences in these parameters give rise to significant differences in damage effects [18–22]. In this paper, theoretical analysis and experiment are used to study the influence of related variables, such as penetration speed and charge, on the damage inflicted on concrete targets from the combined effects of penetration and explosion. Calculation models of the frontal damage depth and volume are established, and they provide a reference for research on damage effects and protection of concrete buildings subjected to penetration and explosion, while also providing a guide for the optimal design and the best performance-price ratio for penetration-explosion warheads.

2. Experimental Setup

By dividing the target destruction process into the two stages penetration and explosion, the different destructive effects can be better understood, the coupled effect of penetration and explosion can be analyzed more accurately, and the experiment and data collection can be facilitated. A 30 mm caliber smoothbore gun was used to conduct the penetration experiments at medium and low speeds; subsequently, charge explosion was carried out with a static explosion field after target penetration to simulate the process of penetration and explosion and study the damage to the concrete structure resulting from both effects.

A 30CrMnSiNi2A solid projectile was used in the penetration experiments, and its material yield strength was 1413 MPa. Because it is challenging to remove the projectile after it penetrates the target and reaches the charge position for the explosion experiment, the projectile features a two-stage detachable design in which the diameter of the projectile gradually decreases (as shown in Figure 1(a)). The length of the projectile is 100 mm, the diameter of the projectile neck is 20 mm, and the diameter of the projectile tail is 14 mm. A groove is designed into the tail of the projectile to facilitate the use of a specially made flat head screwdriver to rotate the projectile after penetration. The shape of the warhead is oval, and the caliber radius head (CRH) is 2.5. The launch of the projectile utilizes the loading method of the aluminum sabot and the bottom push structure (Figure 2), which controls the initial penetration speed of the projectile at 450–700 m/s. In order to simulate the actual damage due to the penetration-explosion projectile, the warhead part was retained after penetration, and the projectile body was rotated and unloaded to carry out an explosion experiment. The actual state of the projectile before and after penetration is shown in Figure 1(b).

A total of 12 concrete targets were used in the experiment, and the experiment was conducted at a field test range. The strength of 7 targets was C35, and the strength of 5 targets was C40. The sizes of the targets were all

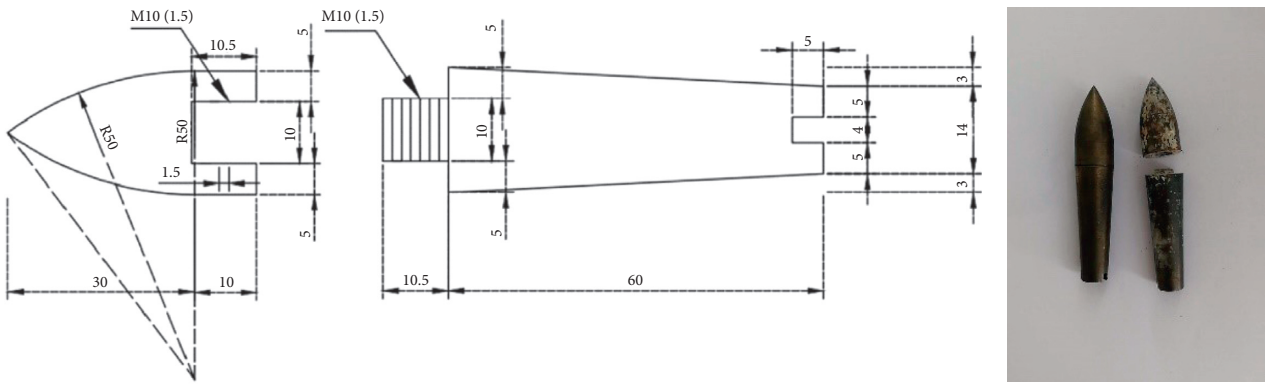

(a) (b)

Figure 1: Penetration projectile (a) design drawing and (b) before and after penetration.

(a) (b)

Figure 2: Aluminum sabot and loading configuration.

ϕ1000 mm × 500 mm. The 8 mm steel hoop is used for circumferential reinforcement to eliminate the radial boundary effect, as shown in Figure 3. The layouts of the experiment site and test equipment are shown in Figures 4 and 5.

The explosion experiment was performed in a static explosion field. The grain was pressed in advance (Figure 6), and the size was ϕ20 mm × 20 mm. The passivated hexogen (RDX) was arranged in the penetration tunnel, and the column charging method was adopted. The arrangement is shown in Figure 7.

3. Results

Concrete impact experiments were performed with different initial penetration speeds, and then the damage status of each target was recorded. A high-speed camera was used to record the target's attitude, and the frames/sec speed of the camera is 4000 FPs. Each bullet had a correct attitude toward the target. Figure 8 shows the attitude of the bullet and the damage inflicted on the target during the penetration experiment on target 5. After the projectile penetrates the

Figure 3: Experimental concrete target.

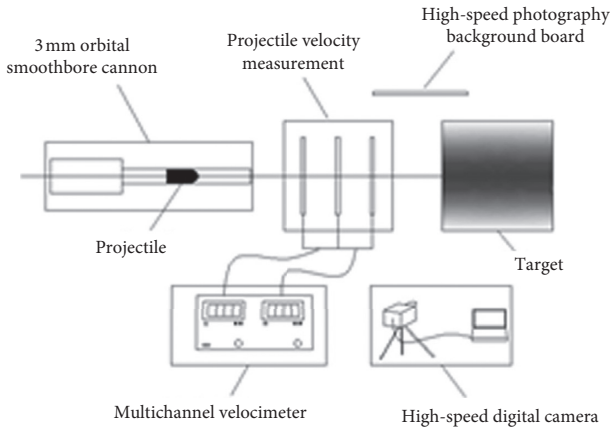

Figure 4: Penetration experiment schematic diagram.

Figure 5: Penetration experiment site.

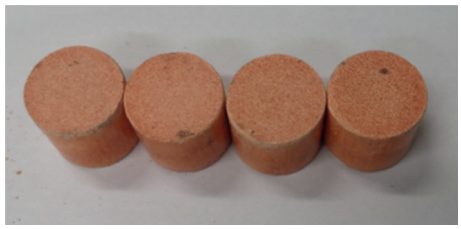

Figure 6: Pressed grain.

Figure 7: Cylindrical charge layout.

target, pits will be formed on the surface of the target. The initial damage state of the target can be judged based on the pit area and the number and size of cracks. The target speed and penetration depth of each projectile were recorded. The data are shown in Table 1.

The penetrated target was transported to a static explosion field for the explosion experiment. After the explosion, a funnel-shaped crater appeared on the front of the target and a few cracks appeared outside the damaged area. The cracks of some targets connected to each other to cause fragmentation in some areas, and some concrete fragments were peeled off from the front of the target. After the explosion, the pits were noticeable, and it was found that the integrity of the target was poor. During the experiment, high-speed photography was used to record the concrete throwing process during the explosion, and the frames/sec speed of the camera is 3000 FPs. Figure 9 shows a concrete throwing image recorded for target 7, when it was subjected to an explosive load. After the experiment, three-dimensional scanning and recording of the target's combined penetration-explosion damage were performed. Figure 10 shows the damage on some targets' blast sides, and Figure 11 shows 3D scans of targets' damaged areas. The explosive used in the explosion experiment was passivated hexogen (RDX) with a density of 1.5 g/cm^3, the explosion heat was 5215 J/g, the detonation velocity was 8150 m/s, and the charge diameter was 20 mm. Other relevant data such as charge, aspect ratio, and target damage status are shown in Table 2.

4. Discussion

Because it is difficult to establish a complete mathematical and mechanical model for combined penetration-explosion damage, dimensional analysis is used for simplification. Determining the relationship between multiple physical quantities is useful for studying the influencing factors and formulating applicable empirical rules [23–25]. In this paper, we adopt the *L-F-T* mechanics system to conduct a dimensional analysis of the combined effects of penetration and explosion.

The main parameters involved in the contact explosion following low- and medium-speed penetration are shown in Table 3 [26–35].

The damage depth is a factor representing the penetration-explosion experiment on the blast site. In addition, the study of the damage shape and volume of the blast side can provide a theoretical basis for damage assessment and the rapid repair and of concrete structures, which is of great significance. Therefore, key parameters are discussed below.

From a physical point of view, the damage depth depends on the parameters related to the material and the geometric characteristics of the projectile [33, 34, 36, 37], explosive, and target, which can be summarized as

$$h_1 = f\left(\rho_e, l_e, d_e, I, E_T, f_T, \mu_T, \rho_T, H, v_d\right). \quad (1)$$

Using the Buckingham theorem [23, 25], equation (1) can be expressed in the following dimensionless form:

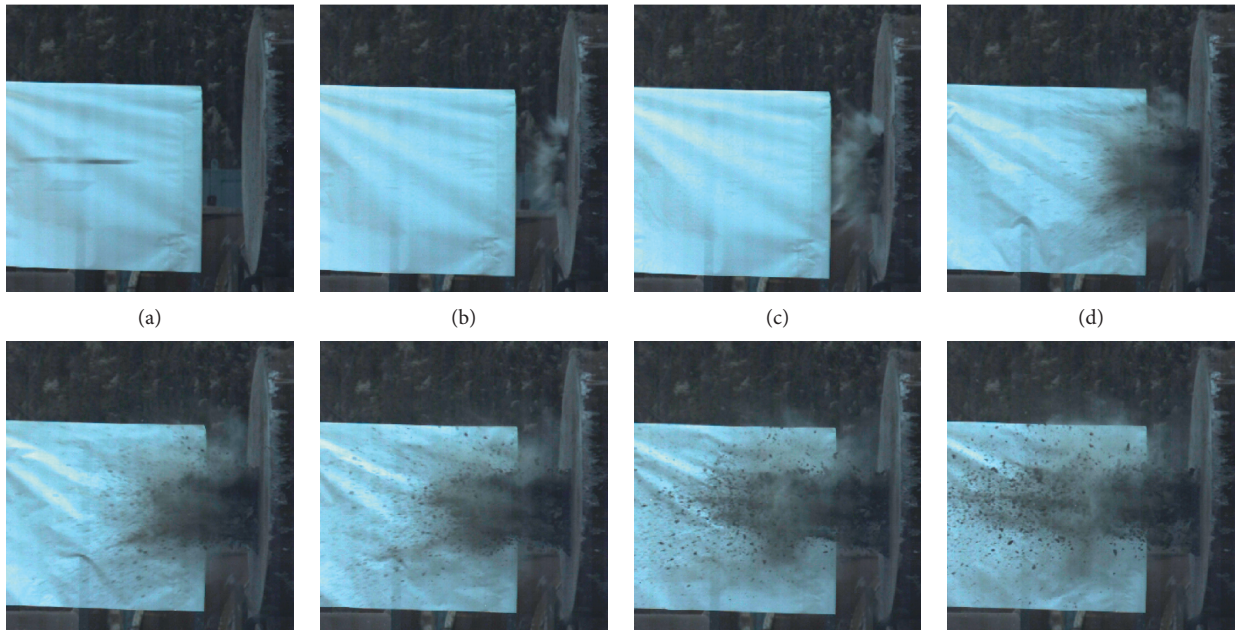

Figure 8: No. 5 shot penetration experiment projectile attitude and concrete throwing image. (a) $t = 0$ s, (b) $t = 0.00125$ s, (c) $t = 0.0025$ s, (d) $t = 0.005$ s, (e) $t = 0.00875$ s, (f) $t = 0.0125$ s, (g) $t = 0.01875$ s, and (h) $t = 0.025$ s.

Table 1: Experimental results of projectile penetrating into concrete targets.

No.	Target type	Penetration speed (m/s)	Projectile mass (g)	Penetration results	
				Penetration depth (m)	States of rear side
1	C30	588.75	168.04	0.275	No change
2		567.47	169.98	0.265	No change
3		548.13	167.85	0.278	No change
4		525.27	167.62	0.231	No change
5		512.37	167.57	0.226	No change
6		488.73	168.04	0.221	No change
7		479.20	168.28	0.211	No change
8	C40	686.86	168.63	0.284	No change
9		612.52	167.61	0.253	No change
10		566.25	167.89	0.234	No change
11		548.82	167.54	0.225	No change
12		446.87	167.97	0.185	No change

$$\frac{h_1}{d_e} = f\left(\frac{\rho_e}{\rho_T}, \frac{l_e}{d_e}, I, \frac{v_d\sqrt{\rho_T}}{d_e \cdot \sqrt{E_T{}^3}}, \frac{H}{d_e}, \mu_T, \frac{f_T}{E_T}\right). \tag{2}$$

The impact energy factor I refers to the definition of the impact coefficient offered by Haldar [4, 38]. This factor is a dimensionless quantity:

$$I = \frac{Nmv^2}{D^3 f_T}, \tag{3}$$

where N represents the shape factor of the warhead, m is the projectile mass, v is the initial penetration velocity, and D is the projectile diameter. In this experiment, some parameters, such as the shape of the warhead, the projectile diameter, the density of the cylindrical charge, and the detonation speed, were held constant. Therefore, the only remaining projectile variables are the initial penetration velocity and projectile mass, and the only remaining explosive variables are the diameter and length of the explosive. For a specific concrete material, the elastic modulus, Poisson's ratio, and density are definite values, the target thickness is also a fixed value, and the impact energy factor already includes the material parameters of the concrete. Therefore, the dimensionless expression for the damage depth after the explosion can be simplified to

$$\frac{h_1}{d_e} = f\left(\frac{l_e}{d_e}, I\right), \tag{4}$$

where the first variable of the above formula is the CAR (charge aspect ratio), an explosion parameter that also represents the size of the charge in this experiment. The second variable is the penetration parameter, which contains the material parameters of the concrete. The relationship

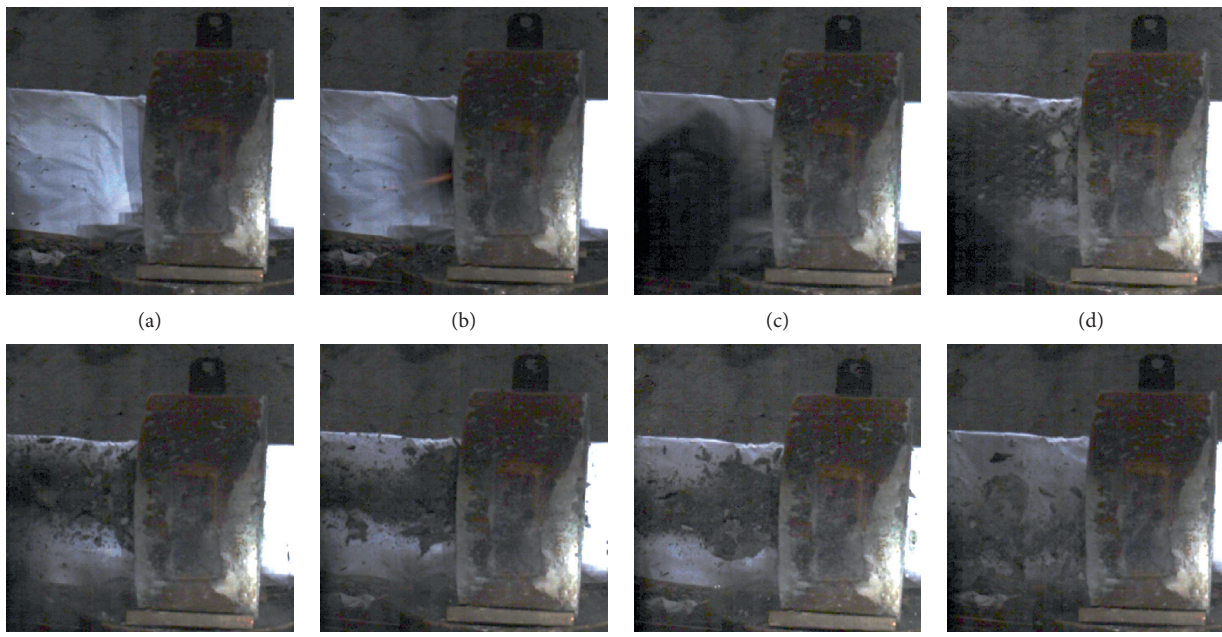

Figure 9: No. 7 explosion experiment and concrete throwing image. (a) $t = 0$ s, (b) $t = 0.001$ s, (c) $t = 0.0025$ s, (d) $t = 0.01$ s, (e) $t = 0.03$ s, (f) $t = 0.075$ s, (g) $t = 0.09$ s, and (h) $t = 0.18$ s.

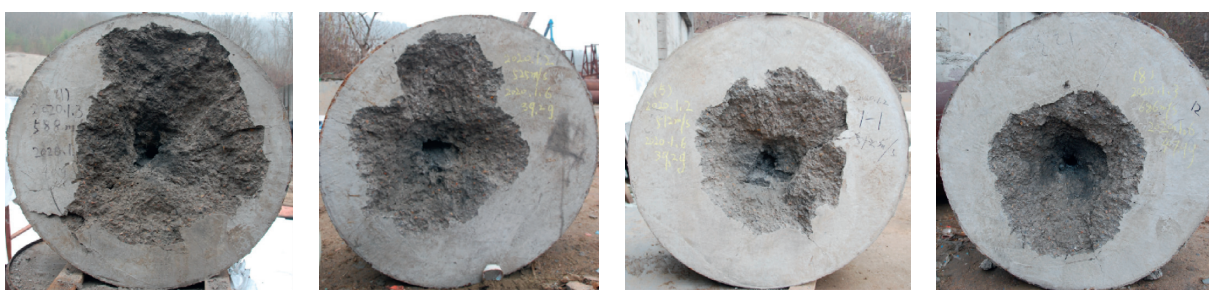

Figure 10: Penetration-explosion damage of concrete targets. (a) Target 1, (b) target 4, (c) target 5, and (d) target 8.

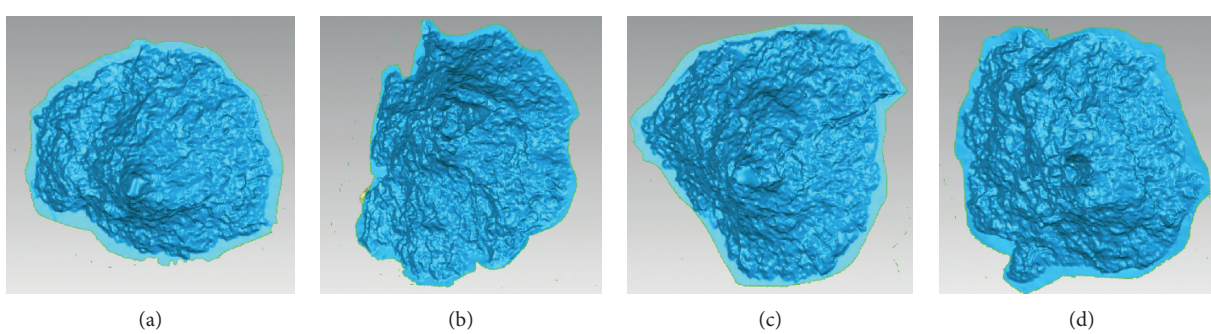

Figure 11: 3D scan of the damaged area. (a) Target 2, (b) target 5, (c) target 9, and (d) target 12.

between the dimensionless damage depth and impact energy factor I is shown in Figure 12.

Analysis of Figure 12 shows that the dimensional damage depth is low when the CAR = 4; it is high when the CAR = 6, while for CAR = 5, it is at an intermediate level. We can make corrections by reasonably assigning adjustments. In fact, as the momentum of the penetration projectile increases, the rate of the increase in penetration depth will taper off. The impact of the initial penetration damage on the explosive load will stabilize, and the increase in the damage

Table 2: Experimental results of penetration-explosion joint damage to concrete targets.

No.	Target type	Charge quality (g)	Charge volume (m^3)	Buried depth (m)	Charge aspect ratio	Results		
						Damage depth (m)	Blast side damage volume (m^3)	States of rear side
1	C30	31.4	2.5132×10^{-5}	0.275	4 : 1	0.302	0.01820	Crack
2		39.25	3.1416×10^{-5}	0.265	5 : 1	0.298	0.01507	Crack
3		47.9	3.7699×10^{-5}	0.278	6 : 1	0.316	0.01203	Spallation
4		39.25	3.1416×10^{-5}	0.231	5 : 1	0.262	0.01198	No change
5		39.25	3.1416×10^{-5}	0.226	5 : 1	0.255	0.01481	No change
6		39.25	3.1416×10^{-5}	0.221	5 : 1	0.246	0.01041	No change
7		39.25	3.1416×10^{-5}	0.211	5 : 1	0.231	0.01004	No change
8	C40	47.9	3.7699×10^{-5}	0.284	6 : 1	0.320	0.01473	Crack
9		39.25	3.1416×10^{-5}	0.253	5 : 1	0.278	0.01037	Crack
10		39.25	3.1416×10^{-5}	0.234	5 : 1	0.255	0.008995	No change
11		39.25	3.1416×10^{-5}	0.225	5 : 1	0.241	0.01199	No change
12		31.4	2.5132×10^{-5}	0.185	4 : 1	0.198	0.009249	No change

Table 3: Governing parameters for thin concrete targets experiencing the combined effects of penetration and explosion.

Parameter	Symbol	Units
Explosive density	ρ_e	FT^2L^{-4}
Explosive length	l_e	L
Explosive diameter	d_e	L
Explosive volume	V_e	L^3
Impact energy factor	I	—
Concrete material elastic modulus	E_T	FL^{-2}
Concrete material strength	f_T	FL^{-2}
Concrete Poisson's ratio	μ_T	—
Concrete density	ρ_T	FT^2L^{-4}
Concrete thickness	H	L
Explosive detonation velocity	v_d	FT^{-1}
Damage depth	h_1	L
Damage volume	V_1	L^3

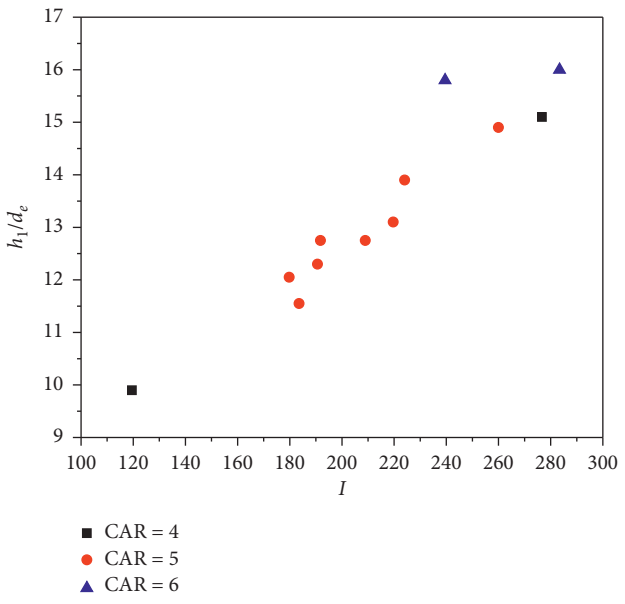

Figure 12: Experimental data at the dimensional damage depth.

depth will also be moderated [6, 39–42]. Finally, the combined load achieves the penetration of the target or maintains a certain damage depth, depending on the relationship between the thickness of the target and the limit of the damage depth. Therefore, it can be assumed that the dimensionless formula equation (4) has a power-type asymptotic representation, which is

$$\frac{h_1}{d_e} = f\left(\frac{l_e}{d_e}, I\right) = \beta\left(\frac{l_e}{d_e}\right)^{\alpha}\left(1 - e^{-\gamma I}\right), \tag{5}$$

where α, β, and γ are constants which are fitted through experimental data to obtain

$$\frac{h_1}{d_e} = 16.5\left(\frac{l_e}{d_e}\right)^{0.111}\left(1 - e^{-0.00536I}\right), \tag{6}$$

$$\text{or}\ \frac{(h_1/d_e)}{(l_e/d_e)^{0.111}} = 16.5\left(1 - e^{-0.00536I}\right). \tag{7}$$

For clarity, the relationship between equation (7) and experimental results is shown in Figure 13. The fitted formula is in good agreement with the experimental results, and the scatter does not exceed the illustrated 10% limits. Of course, this formula has limitations and is only applicable to the data range for the materials used in the experiment although the concrete structures used in this experiment are commonly used in engineering.

Similarly, the damage volume can be obtained by dimensional analysis [23–25]. The parameters related to the damage volume are

$$V_1 = f\left(\rho_e, V_e, d_e, I, E_T, f_T, \mu_T, \rho_T, H, v_d\right). \tag{8}$$

Using the Buckingham theorem [23, 25], equation (8) can be converted into the following dimensionless form:

$$\frac{V_1}{V_e} = f\left(\frac{\rho_e}{\rho_T}, \frac{d_e}{\sqrt[3]{V_e}}, I, \frac{v_d\sqrt{\rho_T}}{\sqrt[3]{V_e}\cdot\sqrt{E_T^3}}, \frac{H}{\sqrt[3]{V_e}}, \mu_T, \frac{f_T}{E_T}\right). \tag{9}$$

The simplified dimensionless expression is

$$\frac{V_1}{V_e} = f\left(\frac{d_e}{\sqrt[3]{V_e}}, I\right). \tag{10}$$

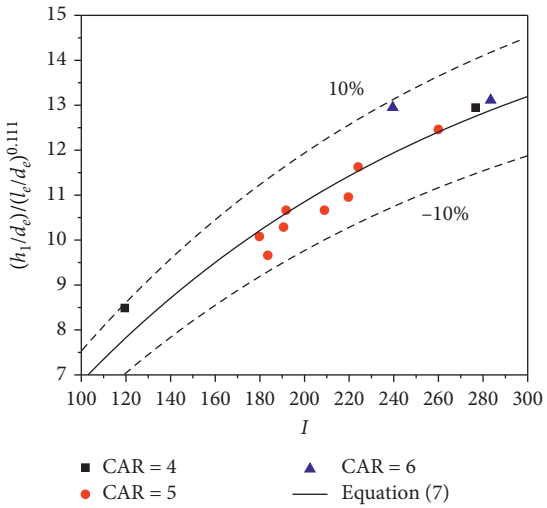

Figure 13: Relationship between equation (7) and experimental results.

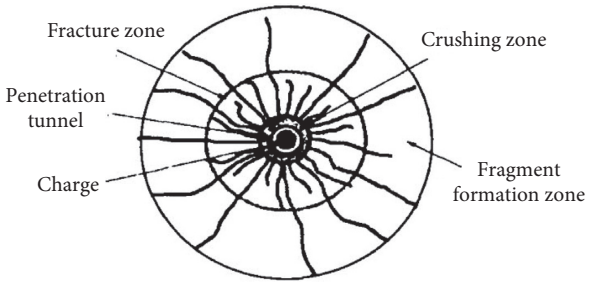

Figure 14: Schematic of crushing zone, fracture zone, and fragment formation zone.

The damage process resulting from the combined penetration-explosion effect is very complicated, and it also exhibits substantial randomness. After the explosive detonated, the surrounding concrete was crushed because of the explosive shock wave. As shown in Figure 14 [43], after the shock wave passed through the crushing zone, it continued to propagate through the surrounding concrete. Since most of the explosive energy is used for crushing and compressing concrete, the energy per unit volume of concrete is reduced. The shock wave is attenuated into a compressive stress wave, which causes compressive strain in the radial direction and tensile strain in the circumferential direction. Due to the high compressive strength and low tensile strength of concrete, many radial tensile cracks are formed in the crushing zone when the tensile stress on the wave front exceeds the tensile strength of the concrete [5]. As shown in Figure 14, the degree of fragmentation in the fragment formation zone, which has the largest impact on cracking, is highly random. This results in a situation in which the damage volumes in Figure 15 are particularly dispersed and substantially irregular.

According to the principles of penetration and explosion damage, it is easy to establish that the growth trend for the damage volume on the blast side of the concrete target is like

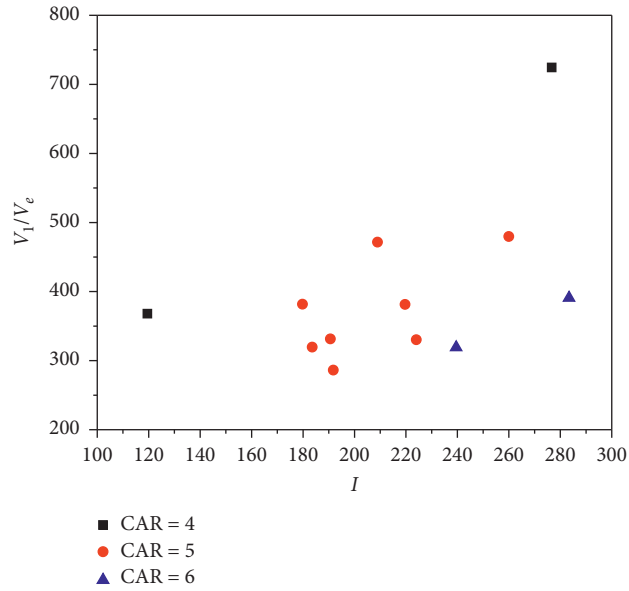

Figure 15: Experimental data in the dimensional damage volume.

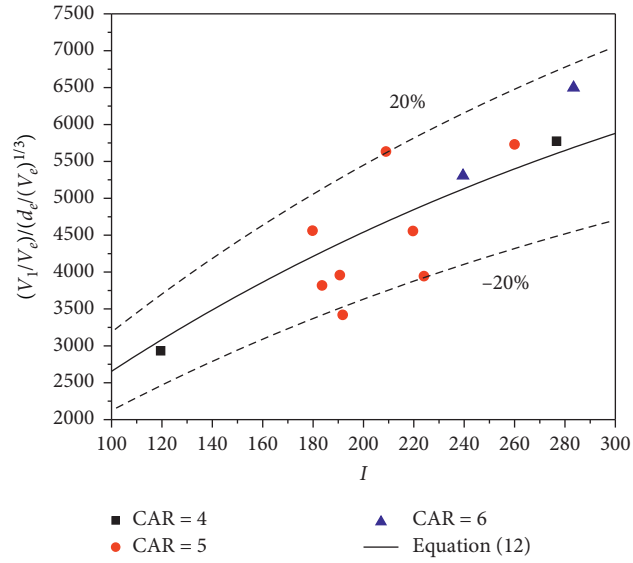

Figure 16: Relationship between equation (12) and experimental data.

the growth trend for the damage depth. As the momentum of the penetrating bullets increases, the increasing ability of the warheads to inflict damage with similar charges will gradually decrease. Therefore, although the study of the damage volume is relatively random, basic relationships can still be drawn for reference. By fitting the experiment results, we obtain

$$\frac{V_1}{V_e} = 9165.27\left(\frac{d_e}{\sqrt[3]{V_e}}\right)^{5.44}\left(1 - e^{-0.00342I}\right), \tag{11}$$

$$\text{or}\ \frac{(V_1/V_e)}{\left(d_e/\sqrt[3]{V_e}\right)^{5.44}} = 9165.27\left(1 - e^{-0.00342I}\right). \tag{12}$$

For clarity, the relationship between the function curve in equation (12) and the experimental results is shown in Figure 16. Due to the large randomness of the experimental results, some data points differ from predicted values by up to 20% of the predicted value. Because there are fewer experimental data (relative to, e.g., Figure 13), this equation is restricted and only provides a theoretical guideline. The randomness of the damage caused by cracks generated by the explosion stress waves is an issue requiring further attention in subsequent studies.

5. Conclusions

This research on the combined effects of penetration and explosion on concrete targets has very important practical significance. Through field experiments, the blast side damage to concrete targets with different penetration speeds and explosive charge conditions is analyzed, and empirical laws and predictions of damage are obtained. This leads to the following main conclusions:

(a) For a given size and quantity of explosives, the damage depth and volume experienced by the concrete target will increase with the increasing impact coefficient of the bullet, but the rate of the increase will gradually diminish. Ultimately, the target will be penetrated or damaged at a constant depth that depends on the relationship between the target thickness and the damage limit.

(b) Using fits to the experimental data for concrete targets, formulas for the damage depth and volume are proposed in equations (6) and (11), and the two equations agree well with experimental data. This establishes the dependence of the damage depth and volume on the aspect ratio (or charge) of the explosive and the kinetic energy of the penetration. Similarly, these equations can provide a guide for the optimal design of penetration-explosion warheads.

(c) The damage volume in concrete targets exhibits substantial randomness and is affected by many factors. The collapse of materials caused by cracks in the fragment formation zone deserves further experimental attention. The unevenness of the aggregate and the random orientation of the cracks may prevent the concrete material from meeting performance expectations. This problem is of considerable significance when considering damage assessment and the rapid repair of concrete structures.

In addition, the combined effect of penetration and explosion will cause the rear side of the concrete structure to collapse, and the internal personnel of the building will cause casualties. The value of critical collapse thickness and the law of damage to the back of the concrete structure are the key issues to be addressed in the following research.

Data Availability

The data used to support the findings of this study are included within the article.

Conflicts of Interest

The authors declare that there are no conflicts of interest regarding the publication of this paper.

Acknowledgments

The authors want to thank Editage for English language editing. This study was funded by the National Natural Science Foundation of China (Grant no. 51808553).

References

[1] G. Wang, S. Zhang, W. Lu et al., "Damage effects of concrete gravity dams subjected to underwater explosion," *Journal of Hydraulic Engineering*, vol. 46, no. 2, pp. 723–731, 2015.

[2] Q. Zheng, Q. Qian, Z. Zhou et al., "Comparative analysis of scabbing thickness estimation of reinforced concrete structures," *Engineering Mechanics*, vol. 20, no. 3, pp. 47–53, 2003.

[3] X. Zhang, X. Yan, Z. Chen et al., "Explosion spalling of reinforced concrete slabs with contact detonations," *Journal of Tsinghua University: Science and Technology*, vol. 46, no. 6, pp. 765–768, 2006.

[4] Q. Zheng, Z. Zhou, Q. Qian et al., "Spallation in protective structures," *Chinese Journal of Rock Mechanics and Engineering*, vol. 22, no. 8, pp. 1393–1398, 2003.

[5] G. Yang, G. Wang, W. Lu et al., "Damage characteristics of concrete structures under the combined loadings of penetration and explosion," *Journal of Central South University*, vol. 48, no. 12, pp. 3284–3292, 2017.

[6] D. J. Frew, S. J. Hanchak, M. L. Green, and M. J. Forrestal, "Penetration of concrete targets with ogive-nose steel rods," *International Journal of Impact Engineering*, vol. 21, no. 6, pp. 489–497, 1998.

[7] Y. L. Xue, D. G. Tang, W. X. Chen, Z. Z. Li, D. P. Li, and M. L. Yao, "Experimental and analytical study on the penetration of corundum-rubble concrete subjected to projectile impact," *Shock and Vibration*, vol. 2017, Article ID 1396567, 10 pages, 2017.

[8] J. Xue, P. Shen, and X. Wang, "Engineering calculation model for a projectile's penetrating into a concrete target with attack angle," *Journal of Vibration and Shock*, vol. 36, no. 13, pp. 238–244, 2017.

[9] D. Zhang, S. Gao, H. Liu et al., "Real-time predicting penetration depth of projectiles into concrete targets based on acceleration measurement and fuzzy model," *Journal of Vibration and Shock*, vol. 36, no. 5, pp. 176–181, 2017.

[10] F. Zhang, L. H. Poh, and M. Zhang, "Critical parameters for the penetration depth in cement-based materials subjected to small caliber non-deformable projectile impact," *International Journal of Impact Engineering*, vol. 137, Article ID 103471, 2020.

[11] C. Liu, X. Zhang, H. Chen, J. Wang, H. Wei, and W. Xiong, "Experimental and theoretical study on steel long-rod projectile penetration into concrete targets with elevated impact velocities," *International Journal of Impact Engineering*, vol. 138, Article ID 103482, 2019.

[12] W. F. Cofer, D. S. Matthews, and D. I. Mclean, "Effects of blast loading on prestressed girder bridges," *Shock and Vibration*, vol. 19, no. 1, pp. 1–18, 2012.

[13] Y. Fu and Q. Zhang, "Study on blasting crater size model in reinforced concrete," *Transactions of Beijing Institute of Technology*, vol. 26, no. 9, pp. 761–764, 2006.

[14] J. Li and H. Hao, "Numerical study of concrete spall damage to blast loads," *International Journal of Impact Engineering*, vol. 68, no. 3, pp. 41–55, 2014.

[15] S. Zhang and G. Wang, "Antiknock performance of concrete gravity dam subjected to underwater explosion," *Explosion and Shock Waves*, vol. 33, no. 3, pp. 255–262, 2013.

[16] T. Rabczuk, J. Eibl, and L. Stempniewski, "Numerical analysis of high speed concrete fragmentation using a meshfree Lagrangian method," *Engineering Fracture Mechanics*, vol. 71, no. 4–6, pp. 547–556, 2004.

[17] B. Leng, J. Xu, H. Sun et al., "Numerical simulation of dynamic response of concrete subjected to internal load of blast," *Chinese Journal of High Pressure Physics*, vol. 23, no. 2, pp. 111–116, 2009.

[18] J. Lai, X. Guo, and Y. Zhu, "Repeated penetration and different depth explosion of ultra-high performance concrete," *International Journal of Impact Engineering*, vol. 84, pp. 1–12, 2015.

[19] D. Yang and X. Wang, "Study on numerical simulation method of explosion in concrete," *Explosion and Shock Waves*, vol. 25, no. 6, pp. 569–573, 2005.

[20] H. Zhang, Z. Duan, L. Yan et al., "Study on the collapse perforation of thick concrete targets under internal explosion," *Transactions of Beijing Institute of Technology*, vol. 33, no. 5, pp. 441–444, 2013.

[21] H. Wen, "Empirical equations for the impact response of concrete targets," *Explosion and Shock Waves*, vol. 23, no. 3, pp. 267–277, 2003.

[22] D. E. Grady, "The mechanics of fracture under high-rate stress loading," in *Proceedings of the Preprints of the William Prager Symposium on Mechanics of Geomaterials: Rocks, Concrete and Soils*, Northwestern University, Evanston, IL, USA, pp. 149–188, 1980.

[23] L. I. Sedov, M. Friedma, and R. E. Street, *Similarity and Dimensional Methods in Mechanics*, Mir Publishers, Moscow, Russia, 1982.

[24] J. Tao and K. Zhang, *Soil Rock Blasting Similarity Law and Blasting Parameter Optimization*, Science Press, Beijing, China, 1998.

[25] P. S. Westine, F. T. Dodge, and W. E. Baker, *Similarity Methods in Engineering Dynamics*, Hayden Book Company, Indianapolis, IN, USA, 1973.

[26] C. W. Lampson, *Explosions in Earth, Effects of Impact and Explosion*, Washington, DC, USA, 1946.

[27] C. B. Morrey, *Underground Explosion Theory, Operation Jangle*, Office of Technical Services, Department of Commerce, Washington, DC, USA, 1952.

[28] R. M. Hmidt and K. A. Holsapple, "Centrifuge crater scaling experiment II. Material Strength Effects," *Centrifuge Crater Scaling Experiment II Material Strength Effects*, Defense Nuclear Agency, Washington, DC, USA, 1979.

[29] K. R. Housen, R. M. Schmidt, and K. A. Holsapple, "Crater ejecta scaling laws: fundamental forms based on dimensional analysis," *Journal of Geophysical Research*, vol. 88, no. B3, pp. 2485–2499, 1983.

[30] P. M. Ghare, D. C. Montgomery, and W. C. Turner, "Optimal interdiction policy for a flow networkflow network," *Naval Research Logistics Quarterly*, vol. 18, no. 1, pp. 37–45, 1971.

[31] K. A. Holsapple and R. M. Schmidt, "On the scaling of crater dimensions: 1. Explosive processes," *Journal of Geophysical Research*, vol. 85, no. B12, pp. 7247–7256, 1980.

[32] K. A. Holsapple and R. M. Schmidt, "A material-strength model for apparent crater volume," in *Proceedings of the Lunar and Planetary Science Conference*, vol. 10, pp. 2757–2777, Houston, TX, USA, March 1979.

[33] R. T. Klinkvort, O. Hededal, and S. M. Springman, "Scaling issues in centrifuge modelling of monopiles," *International Journal of Physical Modelling in Geotechnics*, vol. 13, no. 2, pp. 38–49, 2013.

[34] M. A. Sadovskii, V. V. Adushkin, V. N. Rodionov, and G. N. Startsev, "A method of modeling large cratering explosions," *Combustion, Explosion, and Shock Waves*, vol. 3, no. 1, pp. 73–89, 1967.

[35] R. M. Schmidt, "A Centrifuge Cratering Experiment-Development of a Gravity-Scaled Yield Parameter," *Impact and Explosion Cratering: Planetary and Terrestrial Implications*, pp. 1261–1278, 1978.

[36] V. V. Adushkin and B. D. Khristoforov, "Craters of large-scale surface explosions," *Combustion, Explosion, and Shock Waves*, vol. 40, no. 6, pp. 674–678, 2004.

[37] R. M. Schmidt, "A centrifuge cratering experiment," *LPI Contributions*, pp. 259–266, 1976.

[38] J. L. Drake and L. A. Twisdale, *Protective Construction Design Manual*, Air Force Engineering and Services, Tyndall Air Force Base, FL, USA, 1989.

[39] S. J. Hanchak, M. J. Forrestal, E. R. Young, and J. Q. Ehrgott, "Perforation of concrete slabs with 48 MPa (7 ksi) and 140 MPa (20 ksi) unconfined compressive strengths," *International Journal of Impact Engineering*, vol. 12, no. 1, pp. 1–7, 1992.

[40] A. N. Dancygier, D. Z. Yankelevsky, and C. Jaegermann, "Response of high performance concrete plates to impact of non-deforming projectiles," *International Journal of Impact Engineering*, vol. 34, no. 11, pp. 1768–1779, 2007.

[41] A. N. Dancygier, "Rear face damage of normal and high-strength concrete elements caused by hard projectile impact," *ACI Structural Journal*, vol. 95, no. 3, pp. 291–304, 1998.

[42] A. N. Dancygier and D. Z. Yankelevsky, "High strength concrete response to hard projectile impact," *International Journal of Impact Engineering*, vol. 18, no. 6, pp. 583–599, 1996.

[43] J. Fu and J. Pan, "Analysis and experimental research on blasting mechanism of bottom air column charge," *Journal Of Xi'an University Of Mining and Technology*, vol. 15, no. 1, pp. 21–24, 1995.